

Effects of Nuclear Shells and Angular Momentum in Evaporative Deexcitation*

Jacob Gilat†

Department of Applied Science, Brookhaven National Laboratory, Upton, New York 11973

and

J. Robb Grover

Department of Chemistry, Brookhaven National Laboratory, Upton, New York 11973

(Received 29 October 1970)

A detailed statistical-model analysis has been carried out of recently reported proton and α spectra for the complex nuclear reactions $^{63}\text{Cu} + ^{12}\text{C}$ (55 MeV, lab) and $^{64}\text{Zn} + ^{11}\text{B}$ (43 MeV, lab). In both systems the compound nucleus $^{75}\text{Br}^*$ is formed with the same excitation energy of 50 MeV, but the distribution of angular momentum is expected to be significantly different. Observed differences in the experimental spectra were accordingly interpreted in terms of assumed differing angular momentum distributions. In our calculations it was found possible to achieve agreement with the data within experimental error for plausible but widely differing sets of important but unknown systemic properties, viz., the distribution of angular momentum in the $^{75}\text{Br}^*$, and the level densities to high excitation of the several nuclei involved. However, it was always found necessary to include the effect of the proximity of the closed proton shell at $Z=28$. The behavior of the calculated α emission for individual nuclei shows important differences of detail between reasonable sets of input data, although for all such sets the production ratio [(total protons)/(total α particles)] decreases with increasing angular momentum of the compound nucleus. We feel it is significant that one of the data sets giving satisfactory agreement with experiment included level densities calculated numerically up to the high energies involved using a realistic shell model. These calculations have already been shown to give values in agreement with reliable experimental level densities, which are, however, only available for lower energies. Since additional data on the same system are needed to reduce the ambiguities, specific suggestions for further experiments are offered, and examples of how such experiments can be useful are worked out.

INTRODUCTION

The properties of nuclei excited high into the continuum are poorly known. This is because this region of excitation is accessible only to experiments with complex nuclear reactions, the analysis of which is very complicated, involving large numbers of nuclei, nuclear properties, and reaction pathways. The number of different kinds of experiments that can be done is small compared to the number of unknown properties, so that a given system must always remain underdetermined. Since complete knowledge of such a complex system is out of reach, it is appropriate to ask what can be learned despite the difficulties and how reliable such knowledge may be.

Among the many properties or processes for which information might be sought are (i) level densities as functions of nucleon number (including shell effects), excitation energy, angular momentum, and perhaps isospin and deformation, for several to many neighboring nuclei for each of which the various dependencies may differ; (ii) inverse cross sections (i.e., the several optical-model parameters) for collisions between the particles or photons emitted and the excited residual

nuclei as functions of excitation energy, angular momentum, isospin, deformation, etc., for all of the different nuclei involved; (iii) the nature of the initial projectile-target interaction, which will in general be a mixture of direct reactions, precompound processes, and compound-nucleus formation, and leave several to many excited nuclei, each with its own distribution of excitation energy, angular momentum, isospin, deformation, etc.

In spite of this difficult situation we can take advantage of certain effects arising from the complexity itself to extract useful information. We are dealing with a very large number of open reaction channels connecting states spaced much more closely than the available energy resolution and proceeding with rates much faster than the available time resolution. Only quantities averaged over a sizable fraction of these channels can be accessible to any experiment. Furthermore, most experiments are sensitive to the average ratios of such quantities rather than to their absolute magnitudes. The nuclear properties entering into these averages and ratios vary essentially smoothly as functions of energy, nucleon number, and the other relevant parameters.

Therefore, such averages and ratios extracted from experiments should be meaningful for understanding the systems.

To facilitate the extraction of this information, a well-designed experiment should aim not only at the narrowest possible range of averaging (i.e., best attainable resolution) but also and with equal importance at a clear definition of the limits of this range. Similarly, such an experiment will isolate reasonably well some ratios from the multiplicity of other effects.

In this paper we report a calculative analysis of some recent experimental data to try to assess the problem of extraction of information in the spirit of the above discussion. We chose the experimental data recently published by the Columbia University group,¹ which comes closer than most to fulfilling the above criteria. We address ourselves exclusively to a few features of (i) and (iii), namely, to the possibility of determining the dependence of the level densities on nucleon number, energy and angular momentum, and the distribution in angular momentum of nuclei excited in the initial interaction.

COMPUTER PROGRAM AND INPUT DATA

The computer program used in this investigation is essentially the same as described previously,² but incorporates some improvements and extensions³:

- (1) The capability was provided to follow evaporation chains of emitted neutrons, protons, and α particles in any order.
- (2) Independent level densities are employed at each evaporation step for the products of γ , neutron, proton, and α emission.

Binding energies were obtained where possible from the table of experimental values compiled by Mattauch, Thiele, and Wapstra.⁴ Unknown values were those extrapolated from neighboring known ones and tabulated by Garvey *et al.*,⁵ except that a few adjustments were necessary to achieve self-consistency of the entire set used in our calculations. The values used are given in Table I. No experimental value with cited error greater

than ± 0.3 MeV was used, and except for ⁷²Br and ⁷³Br, no extrapolated value was for a nucleus removed by more than one particle emission from a nuclide for which there was an acceptable experimental value. We therefore feel that residual errors in binding energies should not be large enough to vitiate the calculated results.

Transmission coefficients were calculated from published optical-model parameters⁶ using ABACUS-2.⁷ Whenever the atomic number of the evaporating nucleus changed, a new appropriate set of transmission coefficients was introduced. Since for the mass region dealt with here, no low-energy α penetrabilities have been measured, extrapolation of the α -particle transmission coefficients to 10^{-18} was carried out using parabolic extrapolation in $\log T_l$ versus $\log E$.

We assumed effective γ strengths (ξ_L of Ref. 2) in the range 5×10^{-8} to 7.5×10^{-7} for dipole emission (corresponding to $\Gamma_\gamma \sim 0.1$ to 1.7 eV at the neutron binding energy of ⁸²Br), and 2×10^{-12} to 8×10^{-12} for quadrupole emission.

The distribution of compound nuclei with respect to angular momentum was varied as a "parameter" in the calculations, and is described in more detail in a later section.

The program was made very flexible with reference to level densities and yrast levels because the form of the level density was also used as a major "variable." Values can be computed internally, or read in from cards at appropriate points in the calculation. Internally computed level densities were calculated from the Lang⁸ prescription:

$$\rho(E, J) = \omega(E, M = J) - \omega(E, M = J + 1), \quad (1)$$

$$\omega(E, M) = \omega(E - M^2/[aR], 0), \quad (2)$$

$$\omega(E, 0) = Ke^{2\sqrt{aE}}/(R^{1/2}a^2t^3), \quad (3)$$

$$U = E - \delta. \quad (4)$$

Here, $\rho(E, J)$ is the density of levels of spin J at excitation energy between E and $E + dE$, $\omega(E, M)$ is the density of states at the same energy with a projection M of the nuclear-spin vector along some arbitrary quantization axis, a and R are parameters (related, respectively, to the mean density

TABLE I. Mass-excess values used (keV), underlined values from Ref. 4.

	75	74	73	72	71	70	69	68	67	66	65	64	63	62
Br	<u>-69 444</u>	-65 306	-63 448	-58 848	-56 336	-50 748								
Se		<u>-72 212</u>	-68 171	-67 505	-63 175	-61 490								
As			<u>-70 921</u>	-68 219	<u>-67 893</u>	<u>-64 322</u>	-62 819	-57 717						
Ge				<u>-72 579</u>	<u>-69 902</u>	<u>-70 558</u>	<u>-67 101</u>	-66 522						
Ga					<u>-70 135</u>	<u>-68 897</u>	<u>-69 326</u>	<u>-67 074</u>	<u>-66 865</u>	<u>-63 706</u>	<u>-62 658</u>			
Zn						<u>-69 550</u>	<u>-68 425</u>	<u>-69 994</u>	<u>-67 863</u>	<u>-68 881</u>	<u>-65 917</u>			
Cu									<u>-67 291</u>	<u>-66 255</u>	<u>-67 266</u>	<u>-65 428</u>	<u>-65 583</u>	<u>-62 813</u>

and mean square spin projection of the single-particle levels in the nucleus; $aR/2$ can be regarded as the effective nuclear moment of inertia, K is a constant (usually, $K = \frac{1}{12}$), δ is a pairing correction, and the nuclear temperature t is defined by

$$U = at^2 - \frac{\delta}{2}t. \quad (5)$$

This prescription was found to give a better representation of the combinatorial level density at large angular momenta than the formula commonly used⁹:

$$\rho(E, J) = K \frac{(2J+1) \exp[2\sqrt{aU} - (J + \frac{1}{2})^2 / (aRt)]}{(a^3 R^{3/2} t^4)}. \quad (6)$$

A smooth yrast line is implicit in Eqs. (1)–(5):

$$E_J = (J + \frac{1}{2})^2 / aR + \delta. \quad (7)$$

As before, the program is capable of treating the spin-dependent part of the level density and the yrast levels as separate and independent. However, an analysis of shell-model level densities and yrast levels has shown them to be closely related¹⁰; the relationship indicated by that analysis was adhered to throughout this work [i.e., num-

erical yrast values were used with numerical level densities, and Eq. (7) for all other cases].

EFFECTS OF SHELL MODEL ON FEATURES OF EVAPORATION

In the course of the calculations several rather general features or consequences of the statistical model became apparent. Although these matters have a strong bearing on the analysis of data presented in the next section they are sufficiently general to apply to a broad range of other data.

Differential competition between the emission of one type of particle and another as a function of angular momentum and excitation energy is essentially what determines the pattern of deexcitation of highly excited nuclei. As mentioned in the introduction this competition is determined primarily by ratios of nuclear properties, and most importantly by the ratios of nuclear level densities. For this reason we focus on the properties of nuclear level densities, particularly with reference to the shell model.

The relevant properties of nuclear level densities and their effects are illustrated in Figs. 1–4. Each pair of figures illustrates separately the ef-

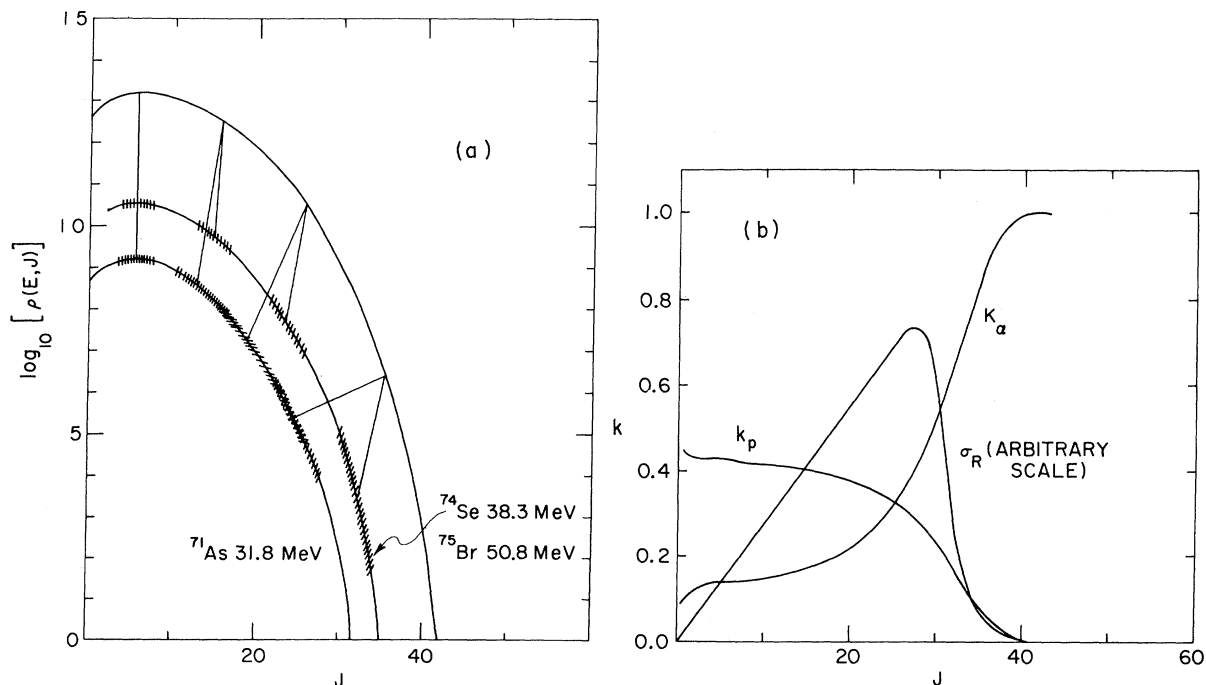


FIG. 1. (a) Level density for ^{75}Br , ^{74}Se , and ^{74}As as a function of angular momentum. The ^{75}Br excitation energy is that of the emitting compound nucleus. For ^{74}Se and ^{74}As , the excitation energy corresponds to mean-energy proton and α emission, respectively. The tie lines represent average proton and α emissions from different angular momenta of the emitting nucleus, and the hatched areas indicate the FWHM of the resulting product distribution. (b) Proton and α -emission probability (averaged over all energies) for the level density above, and total reaction cross section for the $^{63}\text{Cu} + ^{12}\text{C}$ system at 55.9 MeV (lab), all as a function of angular momentum. The parameters used here are $a = A/8$, $R = 2\mathcal{I}_{\text{rigid}}/a$, δ from Ref. 20, and yrast from Eq. (7).

fect of some feature of the level density on the competition between proton and α -particle emission as a function of angular momentum of the emitting nucleus.

Figure 1 illustrates the familiar¹¹⁻¹³ "enhancement" of α -particle emission at large angular momenta. The calculated curves in Fig. 1(a) represent the effective level densities seen by protons and α -particles emitted from ⁷⁵Br at 50.8 MeV, and also the level density of the emitting ⁷⁵Br itself. The points connected by tie lines represent the average proton and α emissions, and demonstrate the respective amounts of angular momentum carried away. As the angular momen-

tum of the emitting nucleus increases, the ability of the α particle to carry away more angular momentum than the proton becomes increasingly more important. At large angular momenta the level density seen by the α particles becomes larger than that seen by the protons, even though the corresponding level-density curve lies always below that seen by the protons. In Fig. 1(b) we see how this reversal affects the emission probabilities of the α particles and protons. The neutron emission probability, not shown here, is similar to that of the protons.

The most important effects modifying this simple picture are consequences of the shell-model

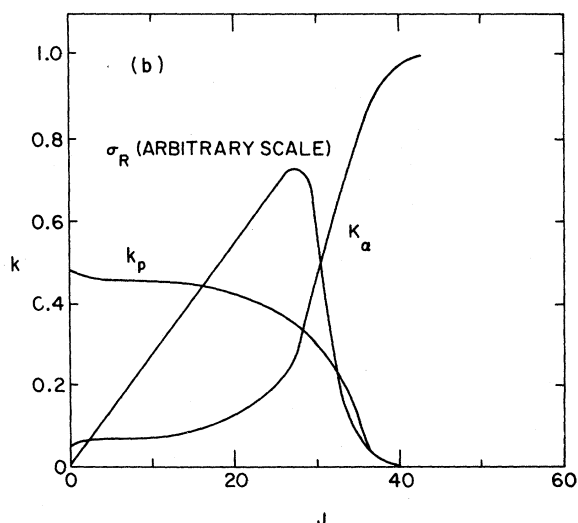
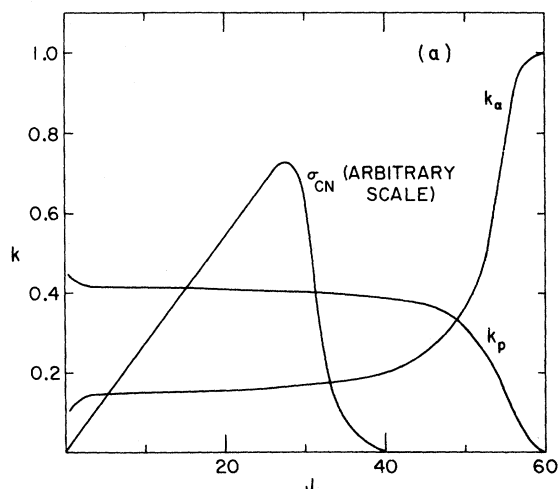
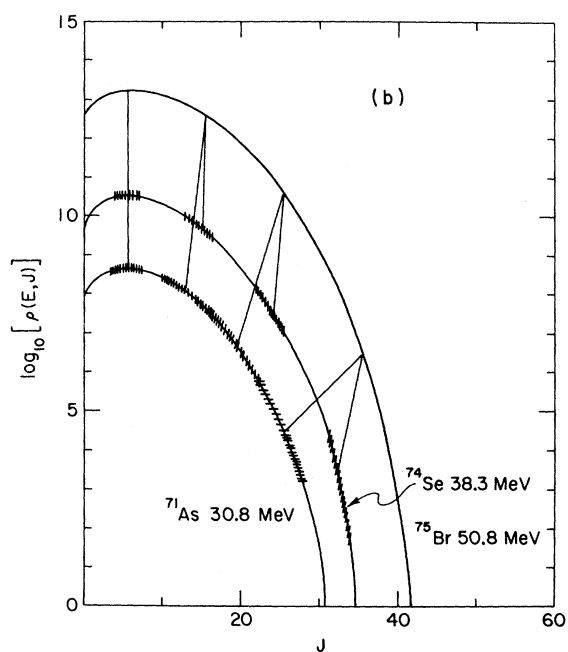
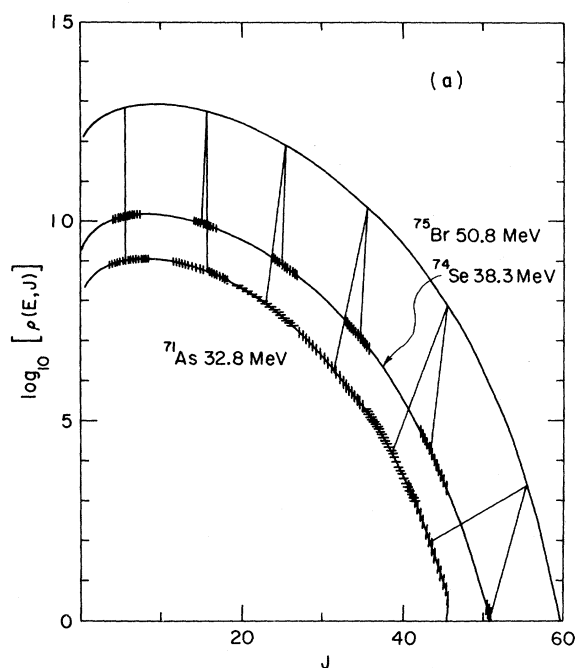


FIG. 2. Same as Fig. 1, for $R = 2 \times (2J_{\text{rigid}}) / a$.

FIG. 3. Same as Fig. 1, for $a(^{71}\text{As}) = A/8 - 0.4$.

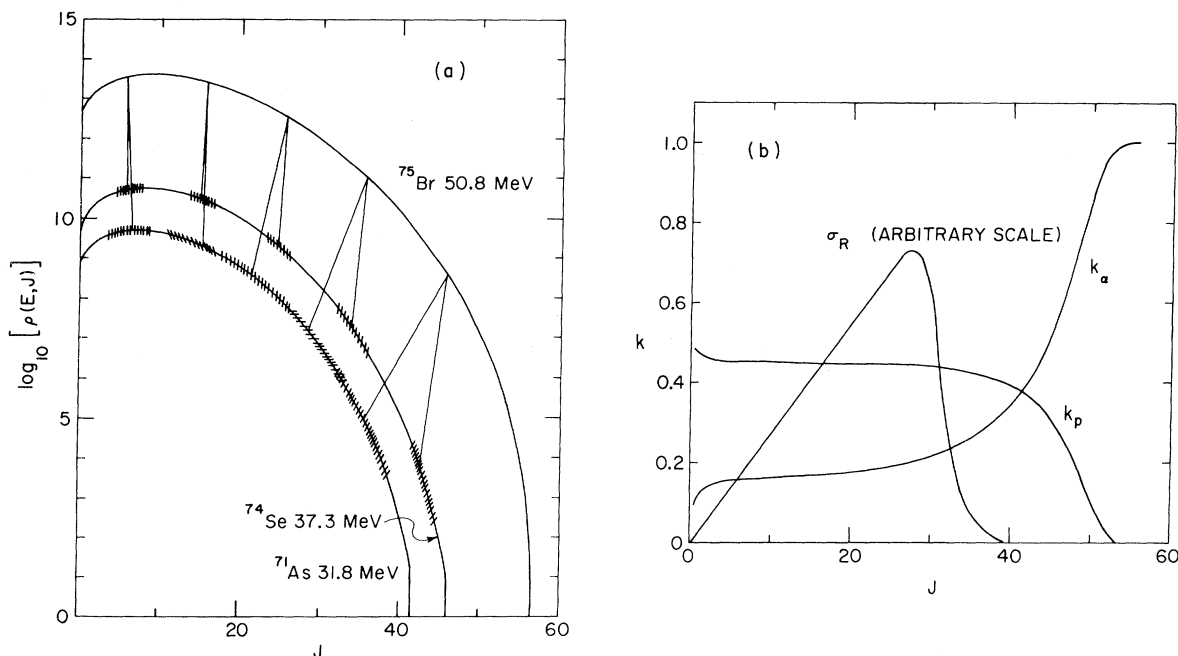


FIG. 4. Same as Fig. 1, for numerical level densities and yrast.

description of the nucleus. Numerical calculations of nuclear level densities in the framework of the shell model have revealed that effective nuclear moments of inertia are often much larger than those corresponding to rigid spheres.^{10, 14} In terms of Eq. (2), this would be reflected in an increased value of R . In Fig. 2 this value has been increased by a factor of 2 with respect to Fig. 1. At large angular momenta the level densities decrease less rapidly with increasing angular momentum. The change that this causes is to increase the angular momentum at which α emission overtakes proton emission. Since the extra amount of angular momentum that can be carried away by α particles relative to protons remains roughly fixed, the effectiveness of the competition of the α particles with the protons hinges upon the steepness with which the respective level densities decrease with increasing angular momentum. In Fig. 2(a) the critical steepness is attained at larger angular momenta than in Fig. 1(a), and the resulting effect on the proton and α emission is shown in Fig. 2(b).

Another consequence of the shell model is the dependence of the parameters (a and R) on nuclear shell structure so that the level density is strongly reduced in approaching a closed shell.^{10, 15, 16} The effect of such a change in a is illustrated in Fig. 3. Here, the α daughter is closer to the 28-proton shell than is the proton daughter, and the level density is correspondingly depressed. (For this case, the effect is exaggerated for illustrative

purposes, but there are cases, such as $n-\alpha$ competition in $^{64}\text{Zn}^*$, in which an effect of this magnitude is realistic.) The main effect here, as shown in Fig. 3(b), is an over-all reduction (by about a factor of 2) of the α -emission probability, especially at low and intermediate angular momenta. The effect would be reversed in going away from a closed shell in α emission.

Finally, in Fig. 4 we show the result of using numerically calculated level densities, in which the effects of Figs. 2 and 3 are mingled. It should be noted that in the numerically calculated level densities the above shell effects persist to high-excitation energies.¹⁴

In realistic situations where successive emissions over a variety of reaction paths must be treated, the consequences of all the effects described above are no longer easy to predict.

The average energies of the emitted particles, especially α particles, are also affected by angular momentum.¹¹ When large amounts of orbital angular momentum are carried away by the α particles emitted from states of high angular momentum, a substantial hardening of their energy spectrum results. For example, the average α energy corresponding to Fig. 1(b) is 15.1 MeV, while that corresponding to Fig. 2(b) is 13.3. (Note that the same values of a are used for both calculations.)

The effect of competition between γ rays and particle emission, seen to be important in other systems,² remains to be discussed. In Figs. 1-4

we see that k_α rises to 1.0 in the neighborhood of the appropriate yrast levels. This behavior is in apparent contrast with that calculated for k_α at 20 MeV in ^{153}Dy (and neighboring nuclides), where γ -ray emission is sufficiently competitive to check the rise of k_α and cause it to decrease again with increasing angular momentum. Actually, these are two aspects of the same picture. It is clear that at some energy, reached in this calculation but not in that of Ref. 2, the γ cascade band terminates. This termination is shown for ^{74}Se in Fig. 5. At small angular momenta the width of the γ cascade band is about 12 MeV, the binding energy of a neutron. As the angular momentum increases its width decreases, finally "pinching off" at approximately $J=27$. For the calculation corresponding to Fig. 4 the "pinchoff" is shifted to a larger angular momentum, $J \approx 40$. (Additional calculations on the Dy system have allowed us to demonstrate the existence of a termination there, also.)

Generally speaking, this terminator will occur at an angular momentum such that α -particle emission from the yrast levels is not too strongly hin-

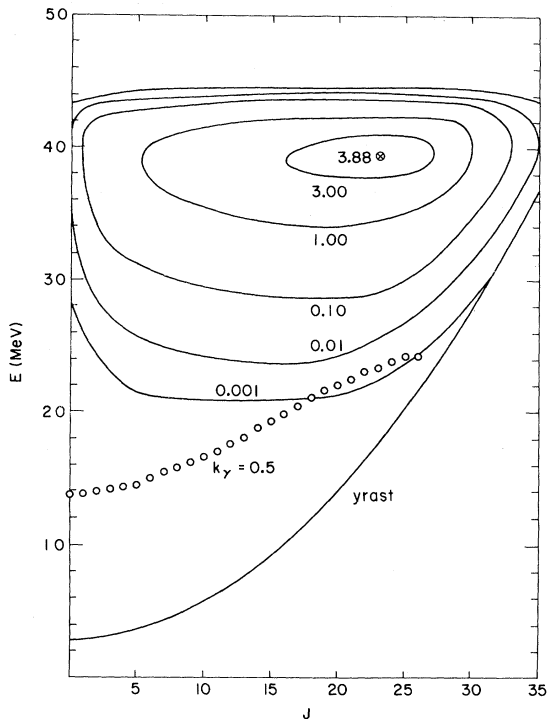


FIG. 5. "Pinchoff" of γ cascade band for ^{74}Se . The solid line represents the locus of yrast levels, circles show the energy and spin at which γ emission reaches 50%. The contours give the distribution of population of the ^{74}Se nucleus as a result of proton emission from ^{75}Br . The parameters used for the calculation are the same as in Fig. 1.

dered. Thus, the energy at which it appears increases with atomic number until, in heavy nuclei, fission becomes more important than α emission in bringing about the termination.

COMPARISON WITH EXPERIMENT

The data selected for detailed comparisons¹ consist of measurements of differential cross sections with respect to energy and angle of emitted protons and α -particles for the systems $^{63}\text{Cu} + ^{12}\text{C}$ at 55 ± 2 MeV (lab) and $^{64}\text{Zn} + ^{11}\text{B}$ at 43 ± 2 MeV (lab). The compound nucleus for both systems is $^{75}\text{Br}^*$ excited to 50 ± 2 MeV, but it is expected that the distributions with respect to angular momentum are different. In addition, the two may differ in

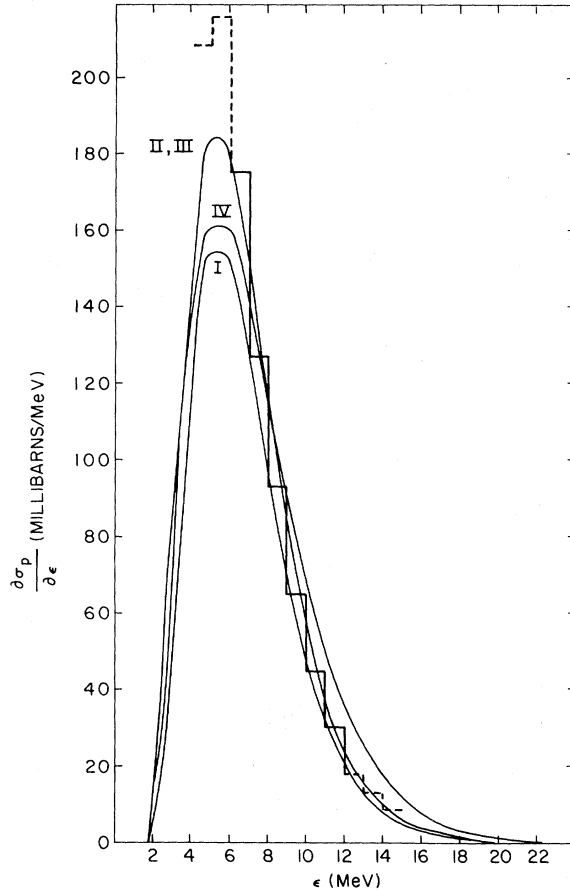


FIG. 6. Calculated and experimental proton spectra for $^{63}\text{Cu} + ^{12}\text{C}$. Histogram—experimental data from Ref. 1. (I) $a=A/8, R=2\sigma_{\text{rigid}}/a, \delta$ from Ref. 20, full J distribution; $\Gamma_\gamma = 1.74$ eV. (II) $a=A/8, R=2\sigma_{\text{rigid}}/a, \delta$ from Ref. 20, J distribution truncated at $\frac{5A}{2}$; $\Gamma_\gamma = 1.74$ eV. (III) $a=A/8, R=2\sigma_{\text{rigid}}/a, \delta$ from Ref. 20, shell corrections of 0.5, 0.75, 1.0, 1.5, and 2.0 MeV for $Z=33, 32, 31, 30$, and 29, respectively; $\Gamma_\gamma = 0.3$ eV. (IV) numerical level density, full J distribution scaled by 0.685; $\Gamma_\gamma = 0.1$ eV.

the distribution of the total reaction cross sections between direct and compound-nucleus processes. The authors of the above work extracted the contribution from the compound-nucleus mechanism to the reaction by reliance on emission into the backward hemisphere in the center-of-mass system.

Figures 6-8 show some of our calculated spectra compared with experiment. All calculations were carried out for $^{75}\text{Br}^*$ excited to 50.8 MeV. Figure 6 displays four proton spectra for the system $^{63}\text{Cu} + ^{12}\text{C}$ calculated using widely different assumptions of level densities and distributions of population in angular momentum. The most notable feature is the nearly stationary character of all these spectra, both in magnitude and shape. The magnitudes of these calculated spectra exceed experiment by a factor of ~ 1.4 if all reactions are assumed to proceed through a compound nucleus. We therefore utilize the insensitivity of the proton spectra to provide a scale factor of 0.7 throughout the calculations. This value for σ_{CN}/σ_R does not seem unreasonable, in view of available experimental information.¹⁷

Figure 7 shows the calculated α spectra corresponding to the proton spectra of Fig. 6. Sensitivity to input parameters here affords a basis for discrimination. The situation is similar for $^{64}\text{Zn} + ^{11}\text{B}$,

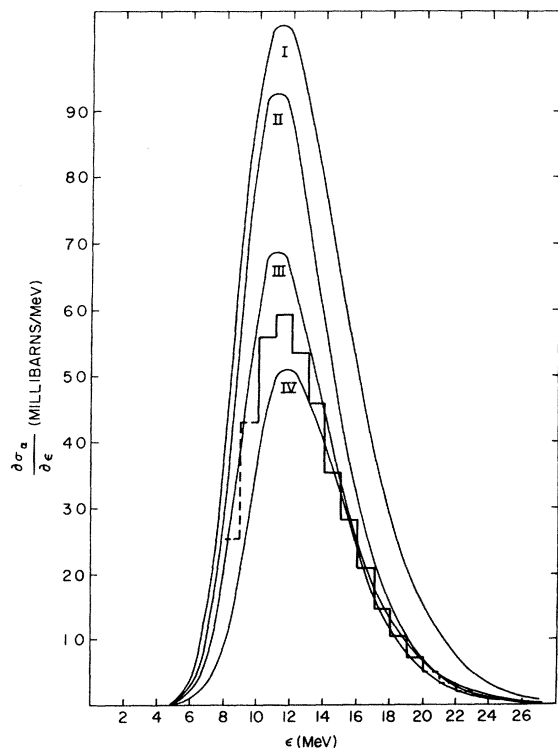


FIG. 7. Calculated and experimental α spectra for $^{63}\text{Cu} + ^{12}\text{C}$. Same notation as in Fig. 6.

as shown in Fig. 8. More information is given in Table II, which presents integrated cross sections and average energies over the energy regions sampled in the experiment, for the same set of calculations.¹⁸

We see that the calculated cross sections in two of the four calculations shown agree with experiment within about 10%. In view of the results of many published calculations for similar data, this agreement is remarkable. It is disquieting, however, that it is achieved for two such disparate sets of assumptions. On the other hand, we are reassured somewhat to see that one of these is the assumption of numerically computed shell-model level densities (IV). This helps support the shell model as an adequate basis for calculating realistic level densities.¹⁹

Calculation III, which results by a small margin in the best over-all agreement with experiment of the four calculations tried is based on a number of quite arbitrary assumptions, consciously chosen according to the various factors described in connection with Figs. 1-4. Three interacting assumptions are involved: (i) The effective moment of inertia was kept small (rigid-body value) and constant. (ii) The distribution of compound nuclei with respect to angular momentum was abruptly truncated at the value dictated by our assumed

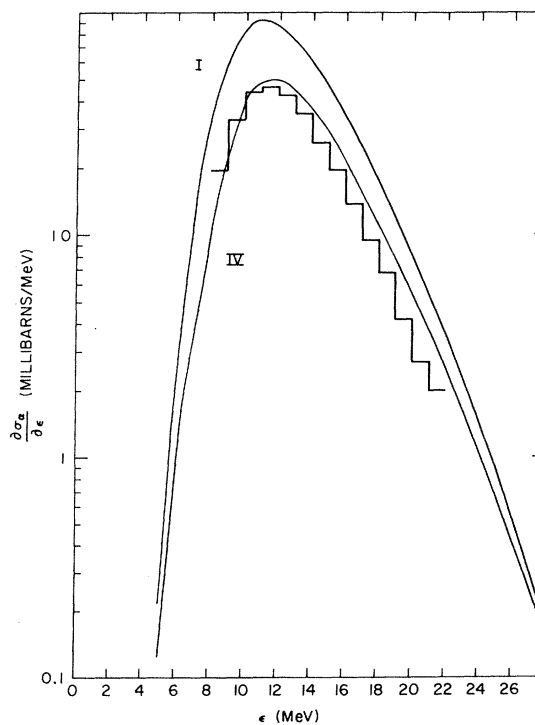


FIG. 8. Calculated and experimental α spectra for $^{64}\text{Zn} + ^{11}\text{B}$. Same notation as in Fig. 6.

TABLE II. Integrated cross sections and average particle energies in the $^{63}\text{Cu} + ^{12}\text{C}$ system (in millibarns and MeV, respectively).

	10-20 MeV		α particles 8-22 MeV		Total		6-12 MeV		Protons 4-14 MeV		Total	
	σ	$\bar{\epsilon}$	σ	$\bar{\epsilon}$	σ	$\bar{\epsilon}$	σ	$\bar{\epsilon}$	σ	$\bar{\epsilon}$	σ	$\bar{\epsilon}$
I	625	13.60	782	13.02	834	12.98	449	8.08	769	7.07	893	6.77
II	500	13.02	601	12.51	633	12.39	536	8.08	921	7.07	1068	6.77
III	359	13.23	449	12.60	472	12.48	544	8.09	929	7.09	1098	6.73
IV	306	13.60	360	13.24	375	13.32	560	8.29	925	7.44	1125	7.15
Exp.	330	13.40	407	12.83	535	8.07	993	6.91

scale factor of 0.7. These two assumptions affect the α -emission probability in opposite directions. (iii) Level-density parameters assumed were $a=A/8$, with pairing energies taken from the literature²⁰; and shell effects of arbitrarily chosen magnitude were introduced through energy adjustments as suggested in Ref. 16. Obviously this is not the only set of such assumptions that could lead to a good fit of the experimental data.

However, we have noticed that all solutions constructed in this way share the common necessity to invoke in some way shell effects on the nuclear level densities. In fact, with the constraint that the nuclear level densities vary reasonably smoothly from nucleus to nucleus it does not seem possible to avoid such shell effects. This provides a strong argument for the persistence of shell effects in nuclear level densities to excitation energies of a few tens of MeV.²¹

We are now in a position to use the additional information provided by comparison of the systems $^{63}\text{Cu} + ^{12}\text{C}$ and $^{64}\text{Zn} + ^{11}\text{B}$ to attempt to reduce the above ambiguities. This is because the observed effects are of the order 20-30% while the theory appears able to deal reasonably with experimental data to within 10%. Since III invokes an arbitrary truncation of the angular momentum distribution, meaningful comparisons of the two systems with this assumption (ii) cannot be made. We therefore limit the comparisons to calculations I and IV, shown in Table III.

Here we see that IV agrees as well with the data of $^{64}\text{Zn} + ^{11}\text{B}$ as it does with that of $^{63}\text{Cu} + ^{12}\text{C}$. Agreement with the experimental effect of angular

momentum, shown in the last row, seems somewhat equivocal but is not outside the combined experimental error and expected closeness of theoretical fit. Aside from further confirmation of IV, we find that the increase in information contributed by the second system is disappointingly small, traceable to the smallness of the effect compared with the uncertainties to be resolved.

However, the great abundance of details available in the calculations may be utilized to select those experiments that will be most effective in resolving ambiguities. A decomposition of the total spectra for calculations III and IV into contributions from individual nuclides is shown in Tables IV and V, which show the angle integrated spectra (in millibarns) and averaged energies (in MeV), broken down according to the atomic number of the emitting nucleus and to the sequential number of the particle emission in the evaporation cascade. We see at once in both cases that the total spectrum is made up of contributions from a wide variety of sources, not dominated by emission from any single nuclide. Even first-chance emission, where all the cross section is concentrated on one nucleus, contributes no more than 30-50%. The average particle energies associated with the different sources vary over a very wide range. A comparison of the individual components reveals some striking differences between calculations III and IV. α emissions from selenium and arsenic in the third step (mainly ^{73}Se and ^{70}As) are affected most strongly. The explanation for this effect is rather complex and involves an interaction of the various effects described in con-

TABLE III. p/α cross section ratios for $^{12}\text{C} + ^{63}\text{Cu}$ and $^{11}\text{B} + ^{64}\text{Zn}$.

	$\frac{\sigma_p(6-12 \text{ MeV})}{\sigma_\alpha(10-20 \text{ MeV})}$			$\frac{\sigma_p(4-14 \text{ MeV})}{\sigma_\alpha(8-22 \text{ MeV})}$			$\frac{\sigma_p(\text{total})}{\sigma_\alpha(\text{total})}$		
	I	IV	Exp.	I	IV	Exp.	I	IV	Exp.
$^{64}\text{Zn} + ^{11}\text{B}$	1.02	1.97	2.01	1.39	2.71	3.09	1.53	3.15	...
$^{63}\text{Cu} + ^{12}\text{C}$	0.72	1.82	1.61	0.98	2.55	2.44	1.07	2.97	...
[Zn/Cu]	1.41	1.08	1.24	1.41	1.06	1.26	1.43	1.06	...

TABLE IV. Breakdown of α emission. [Upper entry in each set is cross section (mb), lower entry is average energy (MeV).]

Step	Calculation III						Calculation IV					
	Br	Se	As	Ge	Ga	Total	Br	Se	As	Ge	Ga	Total
1	161.69					161.69	176.46					176.46
	14.04					14.04	14.45					14.45
2	91.07	71.32	32.81			195.20	54.17	87.32	20.36			161.85
	12.89	12.62	12.02			12.65	13.06	12.89	12.24			12.86
3	7.92	50.38	41.15	11.31	1.79	112.55	3.79	14.68	7.35	9.55	0.25	35.62
	10.69	10.51	9.70	9.24	8.64	10.07	10.67	10.38	9.96	9.30	9.31	10.03
4	3×10^{-3}	0.76	1.48	0.36	0.02	2.62	4×10^{-4}	1.02	0.25	0.27	10^{-3}	1.54
	7.39	7.86	7.66	7.28	6.52	7.65	7.38	7.86	7.19	6.99	6.65	7.58
Total	260.68	122.46	75.44	11.67	1.81	472.06	234.42	103.02	27.96	9.82	0.25	375.47
	13.54	11.72	10.67	9.17	8.62	12.48	14.07	12.48	11.59	9.24	9.31	13.32

nection with Figs. 1–4. More details concerning the deexcitation of ^{70}As are shown in Figs. 9 and 10. Figure 9 shows plots of α -emission probability k_α for a number of excitation energies. In both cases there are curves showing structures similar to those described in Ref. 2 in connection with sub-barrier α emission; i.e., below about 20 MeV the increase of k_α is limited by competition with γ -ray emission. The onset of the termination of the γ -cascade band, discussed above, is apparent at the higher energies. However, k_α is much larger, especially at high angular momentum, for calculation III than it is for calculation IV. This can be understood by reference to the yrast levels assumed in the two calculations (see Fig. 10). The numerical yrast lines are ragged, and display a larger shell effect than the lines assumed in calculation III. The most important difference though is the much larger effective moment of inertia of the numerical values. We can see how this difference causes the large difference in α -emission

probability by considering the deexcitation of nuclei excited to 20 MeV at $J=20$, which in both cases is reasonably near the peak of the respective population distributions. The circles show the mean excitation energy left after emission of the protons and α particles. We see that in calculation III both points fall below their respective yrast lines, i.e., in the “forbidden” region of the E - J plane. Therefore emission of both requires that orbital angular momentum be carried away; 4 units for the protons and 7 for the α particles, and α emission will then be preferred. In calculation IV the proton point falls well above the yrast line while the α point falls below, and of course proton emission is preferred. Thus the difference in moment of inertia is the controlling factor in causing the difference, but a close comparison of the crossover behavior of the two yrast lines in each case shows that the effects already described are enhanced by the shell effect.

Radiochemical measurements seem naturally

TABLE V. Breakdown of proton emission. [Upper entry in each set is cross section (mb), lower entry is average energy (MeV).]

Step	Calculation III						Calculation IV					
	Br	Se	As	Ge	Ga	Total	Br	Se	As	Ge	Ga	Total
1	376.38					376.38	417.95					417.95
	8.27					8.27	8.99					8.99
2	193.14	74.61	51.53			319.28	141.57	91.46	77.97			311.00
	7.19	6.98	6.65			7.05	7.79	7.60	7.16			7.58
3	92.95	139.90	93.13	13.72	5.21	344.91	131.26	77.61	107.35	22.05	9.36	347.63
	5.69	5.40	4.81	4.67	4.10	5.27	5.54	5.03	4.71	4.48	4.28	5.07
4	2.65	41.53	5.44	7.37	0.44	57.43	1.38	37.45	5.20	4.09	0.30	48.42
	3.59	3.69	3.36	3.24	2.93	3.59	3.41	3.56	3.21	3.07	3.01	3.47
Total	665.12	256.04	150.10	21.09	5.65	1098.00	692.16	206.52	190.52	26.14	9.66	1125.00
	7.57	5.58	5.38	4.17	4.01	6.72	8.08	5.90	5.67	4.26	4.24	7.15

sued for distinguishing among alternatives such as calculations III and IV. It is, therefore, of interest to calculate the expected radiochemical cross sections, and these are shown in Table VI. Differences roughly corresponding to the differences in Tables IV and V are indeed evident; e.g., the difference in α emission from $^{70}\text{As}_{37}$ is clearly seen in the cross section²² for $^{66}\text{Ga}_{35}$. Obviously the correspondence cannot be straightforward because in general more than one path of formation is available for a given product, and the effects of different assumptions on the different paths often counteract each other. Also it must be borne in mind that Table VI is calculated for a single bombarding energy, while in general many of the cross sections shown may be strongly energy de-

pendent in the neighborhood of the excitation energy considered. One ought therefore to compare complete excitation functions rather than isolated cross sections. However, as shown in the last column of Table VI the differences found here do not wash out when the isotopic cross sections are added up to form the elemental cross sections, thereby removing most of the energy dependence.

More detailed relationships between the ratios of cross sections displayed in Table VI and the assumptions made in the calculations can be seen in the computer output, but will not be described further here. Suffice it to say that radiochemical measurements on this system appear well justified.

Other types of measurement possibly effective for distinguishing contributions from components or reaction paths would be worthwhile, for example the α - α coincidence rate. Table VII gives the breakdown according to multiplicities for calculations III and IV of α -emission cross sections. We find that in calculation IV the $^{75}\text{Br} \rightarrow ^{71}\text{As} \rightarrow ^{67}\text{Ga}$ α - α cascade contributes about 50% to the total α - α coincidence spectrum. Rates and energy spectra for such coincidence studies are complemen-

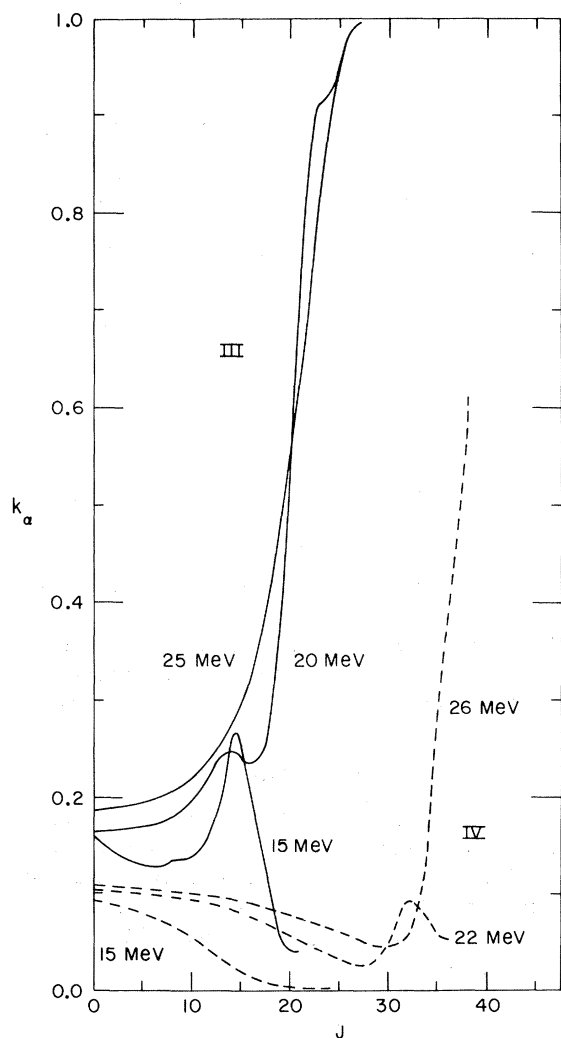


FIG. 9. Values of α -emission probability k_α calculated for ^{70}As . Solid: calculation III; dashed: calculation IV.

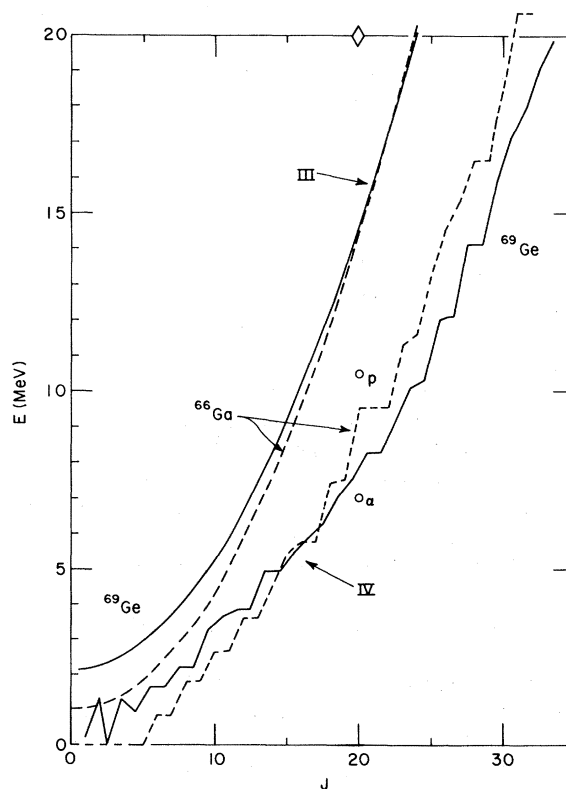


FIG. 10. Yrast values used in calculations III and IV, for ^{69}Ge (solid) and ^{66}Ga (dashed). The open points show approximately the mean excitation energy left after emission of a proton and an α particle from ^{70}As at $J=20$ excited to 20 MeV (represented by a diamond).

TABLE VI. Calculated radiochemical cross sections (mb) $^{63}\text{Cu} + ^{12}\text{C}$ ($E_x = 50.8$ MeV).

$Z \backslash N$		40	39	38	37	36	35	34	33	32	Total
^{35}Br	IV		0.014	5.77	3.06						8.8
	III		0.003	2.19	7.62						9.8
^{34}Se	IV	0.034	41.51	339.23	1.71						382
	III	0.01	20.76	260.49	5.36						287
^{33}As	IV	10.84	122.85	44.68	22.26	21.71	7×10^{-4}				222
	III	4.98	180.89	55.85	20.37	29.08	7×10^{-3}				291
^{32}Ge	IV	23.40	2.15	47.64	177.32	6.98					257
	III	4.98	3.77	24.42	202.61	4.01					240
^{31}Ga	IV	4×10^{-3}	0	23.40	5.33	5.72	9.71	0.05			44
	III	2×10^{-3}	0	17.18	9.48	10.17	52.16	0.09			89
^{30}Zn	IV			6×10^{-3}	0	18.90	0.56				19
	III			2×10^{-3}	0	16.52	0.80				17
^{29}Cu	IV					10^{-3}	0	0.25	10^{-4}		0.25
	III					2×10^{-3}	0	1.79	0.02		1.8

TABLE VII. Calculated rates of α - α coincidence (in mb).

	Calculation III			Calculation IV		
	Singles only	Doubles only	Triples only	Singles only	Doubles only	Triples only
^{75}Br	107.4	52.5	1.8	148.8	27.5	0.25
^{74}Br	70.6	20.5		52.0	2.2	
^{73}Br	7.9	0.02		3.8	0.01	
^{74}Se	64.7	6.7		82.1	5.2	
^{73}Se	50.4	0.1		14.6	0.04	
^{72}Se	0.8			1.0		
^{73}As	4.2			2.4		
^{72}As	1.4			0.2		
Total	307.3	79.8	1.8	304.9	35.0	0.25

tary to the radiochemical information, which is not available for all the products, and which cannot give spectral information. Much the same can be said for other types of coincidence experiments, (p, α), (γ, α), etc. In particular, gating of particle spectra on a well-defined γ transition near the ground state of some product nucleus should be very helpful.

We have not yet extended our calculations to include angular distributions of emitted particles, although the available experimental information could be highly useful. The angular distribution should reflect any tendency of the nucleons and α particles to be emitted from different regions of

angular momentum, as suggested in Figs. 1(b)-4(b).

Also, as is already being done for a few systems,^{23,24} the compound-nucleus contribution to the total reaction cross section should be measured.

ACKNOWLEDGMENTS

We are grateful to Dr. R. C. Reedy for communicating experimental data to us prior to publication. One of us (J.G.) thanks the Department of Applied Science, Hot Laboratory Division, Brookhaven National Laboratory, and Dr. Manny Hillman for kind hospitality.

*Work performed under the auspices of the U. S. Atomic Energy Commission.

†Present address: Israel Atomic Energy Commission, Soreq Nuclear Research Center, Yavne, Israel.

¹R. C. Reedy, M. J. Fluss, G. F. Herzog, L. Kowalski, and J. M. Miller, *Phys. Rev.* **188**, 1771 (1969), and private communication.

²J. R. Grover and J. Gilat, *Phys. Rev.* **157**, 802 (1967).

³J. Gilat, Brookhaven National Laboratory Report No. BNL 50246 (T-580), 1970 (unpublished).

⁴J. H. E. Mattauch, W. Thiele, and A. H. Wapstra, *Nucl. Phys.* **67**, 1 (1965).

⁵G. T. Garvey, W. J. Gerace, R. L. Jaffe, I. Talmi, and I. Kelson, *Rev. Mod. Phys.* **41**, 51 (1969).

⁶F. Bjorklund and S. Fernbach, *Phys. Rev.* **109**, 1295 (1958) for neutrons; F. G. Perey, *Phys. Rev.* **131**, 745 (1963) for protons; J. R. Huizenga and G. Igo, *Nucl. Phys.* **29**, 462 (1962) for α particles.

⁷E. Auerbach, Brookhaven National Laboratory Report No. BNL 6562, 1962 (unpublished).

⁸D. W. Lang, *Nucl. Phys.* **77**, 545 (1966).

⁹The first comprehensive treatment of level density as a function of angular momentum is due to C. Bloch, *Phys. Rev.* **93**, 1094 (1954). He showed that the exponential dependence of Eq. (6) is valid only when one assumes a continuous distribution of single-particle levels and retains only the first term in a series expansion of the resulting equation in powers of J^2 . All subsequent derivations of level density expressions similar to Eq. (6) invoke (or imply) these two assumptions [see T. Ericson, *Advan. Phys.* **9**, 425 (1960); and Ref. 20]. The continuous nature of the single-particle levels is the more basic of the two and is almost a necessary condition for a simple closed level-density formula. The second assumption is more a matter of convenience, and the authors probably never intended to use their expressions beyond a few units of angular momentum, where the first-order expansion is justified and valid. Unfortunately, Eq. (6) has been commonly and indiscriminately applied by most workers in the field to regions of angular momentum for which it was never intended. Hillman and Grover (Ref. 14) used a numerical procedure to solve the combinational level-density problem for a discrete set of single-particle levels. An analysis of their results again shows the importance of higher-order terms at high angular momentum. Lang's prescription, which includes terms of all orders in J^2 , does indeed provide a reasonable description of the numerical results (Ref. 10).

¹⁰J. Gilat, *Phys. Rev. C* **1**, 1432 (1970).

¹¹D. C. Williams and T. D. Thomas, *Nucl. Phys.* **A92**, 1 (1967).

¹²N. D. Dudey and T. T. Sugihara, *Phys. Rev.* **139**, B896 (1965).

¹³D. V. Reames, *Phys. Rev.* **137**, B332 (1965).

¹⁴M. Hillman and J. R. Grover, *Phys. Rev.* **185**, 1303

(1969).

¹⁵T. D. Newton, *Can. J. Phys.* **34**, 804 (1956).

¹⁶N. Rosenzweig, *Phys. Rev.* **108**, 817 (1957).

¹⁷Direct experimental measurements (see Refs. 23 and 24) of the total fusion (compound-nucleus production) cross section for the similar system $^{63,65}\text{Cu} + ^{16}\text{O}$ seem to indicate a somewhat higher value ($\sigma_{\text{CN}}/\sigma_{\text{R}} \approx 0.9$) in this energy range. However, in view of experimental errors and uncertainties in the calculated values of σ_{R} the discrepancy does not seem very serious. As a matter of fact, a somewhat different analysis of the data of Ref. 24 does yield a value of $\sigma_{\text{CN}}/\sigma_{\text{R}} \approx 0.7$ for our case (F. Lanzafame and J. M. Alexander, private communication).

¹⁸Values of Γ_{γ} assumed here sample the entire range covered in our study. The effect of this variation on the total spectra is only a few percent, although some components of the spectra and corresponding radiochemical cross sections are more sensitive.

¹⁹It should be noted that the shell-model level densities used here were derived from one generalized version of shell-model single-particle level spacings, with a unique value of the pairing force strength constant GA , and neglecting effects of deformation and residual interactions other than pairing. Further refinements of the model should lead to an even better agreement with the data, and the search for such an agreement opens up the interesting possibility of extracting true structural information from complex nuclear-reaction data.

²⁰A. Gilbert and A. G. W. Cameron, *Can. J. Phys.* **43**, 1446 (1965).

²¹The existence of such shell effects on nuclear level density has been inferred from neutron-resonance counting and evaporated-particle spectra [see D. W. Lang, *Nucl. Phys.* **26**, 434 (1961); A. G. W. Cameron, *Can. J. Phys.* **36**, 1040 (1958); and Ref. 15]. Others [see M. Blann and G. Merkel, *Phys. Rev.* **137**, B367 (1965)] attempted to use reaction data in the neighborhood of closed shells to distinguish between different mathematical approximations of the model by which the shell effects can be treated.

²²Published [see J. B. J. Read, I. M. Ladenbauer-Bellis, and R. Wolfgang, *Phys. Rev.* **127**, 1722 (1962)] excitation functions for the production of ^{66}Ga and neighboring nuclides in the very similar system $^{59}\text{Co} + ^{16}\text{O}$ are not consistent with the high cross section predicted by calculation III, and provide additional evidence for the validity of the shell-model level densities.

²³L. Kowalski, J. C. Jodogne, and J. M. Miller, *Phys. Rev.* **169**, 894 (1968).

²⁴J. B. Natowitz, *Phys. Rev. C* **1**, 623 (1970).